Biogeosciences Open Access
Discussions EGU

1 **Greenhouse gas production in degrading ice-rich permafrost deposits in northeast Siberia**

2 Josefine Walz[1,2], Christian Knoblauch[1,2], Ronja Tigges[1], Thomas Opel[3,4], Lutz Schirrmeister[4], Eva-Maria
3 Pfeiffer[1,2]
4
5 [1]Institute of Soil Science, Universität Hamburg, Hamburg, 20146, Germany
6 [2]Center for Earth System Research and Sustainability, Universität Hamburg, Hamburg, 20146, Germany
7 [3]Permafrost Laboratory, Department of Geography, University of Sussex, Brighton, BN1 9RH, UK
8 [4]Alfred Wegener Institute Helmholtz Centre for Polar and Marine Research, Periglacial Research
9 Section, 14473 Potsdam, Germany
10 *Correspondence to*: Josefine Walz (josefine.walz@uni-hamburg.de)

11

12 **Abstract**

13 Permafrost deposits have been a sink for atmospheric carbon for millennia. Thaw-erosional processes,
14 however, can lead to rapid degradation of ice-rich permafrost and the release of substantial amounts of
15 organic carbon (OC). The amount of the OC stored in these deposits and their potential to be microbially
16 decomposed to the greenhouse gases carbon dioxide (CO_2) and methane (CH_4) depends on climatic
17 and environmental conditions during deposition and the decomposition history before incorporation into
18 the permafrost. Here, we examine potential greenhouse gas production in degrading ice-rich permafrost
19 deposits from three locations in the northeast Siberian Laptev Sea region. The deposits span a period
20 of about 55 kyr and include deposits from the last glacial and Holocene interglacial periods. Samples
21 from all three locations were aerobically and anaerobically incubated for 134 days at 4 °C. Greenhouse
22 gas production was generally higher in glacial than Holocene deposits. In permafrost deposits from the
23 Holocene and the late glacial transition, only 0.1–4.0% of the initially available OC could be decomposed
24 to CO_2, while 0.2–6.1% could be decomposed in glacial deposits. Within the glacial deposits from the
25 Kargin interstadial period (Marine Isotope Stage 3), local depositional environments, especially soil
26 moisture, also affected the preservation of OC. Sediments deposited under wet conditions contained
27 more labile OC and thus produced more greenhouse gases than sediments deposited under drier
28 conditions. To assess the long-term production potentials, deposits from two locations were incubated
29 for a total of 785 days. However, more than 50% of the aerobically produced and more than 80% of
30 anaerobically produced CO_2 after 785 days of incubation were already produced within the first 134 days,
31 highlighting the quantitative importance of the slowly decomposing OC pool in permafrost. CH_4

Biogeosciences

Discussions

EGU

Open Access

32 production was generally observed in active layer samples but only sporadically in permafrost samples

33 and was several orders of magnitude smaller than CO_2 production.

34

35 Key words: Permafrost carbon, greenhouse gases, incubation, Yedoma, Siberian Arctic

36

1   Introduction

38 Permafrost, i.e. ground that is at ≤ 0 °C for at least two consecutive years (van Everdingen, 2005), may

39 preserve organic matter (OM) for millennia (Ping et al., 2015). The current organic carbon (OC) pool of

40 soils and sediments in permafrost-affected landscapes is estimated to be ~1300 Pg, of which ~800 Pg

41 are perennially frozen (Hugelius et al., 2014). However, warming-induced environmental changes and

42 permafrost degradation could lead to rapid thaw of substantial amounts of currently frozen OM, microbial

43 decomposition of the thawed material, and rising greenhouse gas fluxes to the atmosphere (Natali et al.,

44 2015; Schuur et al., 2015). The changes are expected to be most pronounced in near-surface layers

45 (Schneider von Deimling et al., 2012), but thermo-erosion of ice-rich permafrost, i.e. permafrost with >20

46 vol% ice (Brown et al., 1998), also enables deep thaw of several tens of meters (Schneider von Deimling

47 et al., 2015).

48   Ice-rich permafrost deposits, also called ice complex deposits, accumulated in unglaciated Arctic

49 lowlands. During cold stages, fine grained organic-rich material of polygenetic origin was deposited on

50 predominantly flat plains (Schirrmeister et al., 2013). The deposits are dissected by large ice wedges,

51 which can amount for up to 60vol% (Ulrich et al., 2014). The most prominent ice complex deposits,

52 referred to as Yedoma, accumulated during the late Pleistocene between >55 and 13 ka before present

53 (BP), i.e. during the Marine Isotope Stages (MIS) 3 and 2 (Schirrmeister et al., 2011). Locally, however,

54 remnants of older ice complex deposits of MIS 7 or MIS 5 age are also preserved (Opel et al., 2017;

55 Schirrmeister et al., 2002; Wetterich et al., 2016).

56   The thickness of Yedoma deposits in Siberia (Grosse et al., 2013) and Alaska (Kanevskiy et al., 2011)

57 can reach >50 m. At the time of deposition; rapid sedimentation and freezing incorporated relatively

58 undecomposed OM into the permafrost (Strauss et al., 2017). However, owing to the high ice content,

59 Yedoma deposits are highly susceptible to warming-induced environmental changes, erosion, and

60 ground subsidence following permafrost thaw. Only 30% of the Yedoma region (~416,000 km^2) is

61 considered intact (Strauss et al., 2013) while the other 70% have already undergone some level of

62 permafrost degradation (e.g. Morgenstern et al., 2013). Today, the whole Yedoma region stores 213–

Biogeosciences
Discussions

Open Access

EGU

63 456 Pg of OC, of which 83–269 Pg are stored in intact Yedoma and 169–240 Pg in thermokarst and

64 refrozen taberal deposits (Hugelius et al., 2014; Strauss et al., 2013, 2017; Walter Anthony et al., 2014;

65 Zimov et al., 2006). But, high spatial and temporal variability result in large uncertainties of how much

66 OC is thawed out from degrading ice-rich permafrost deposits and how much of this OC can be

67 microbially decomposed to carbon dioxide (CO_2) or methane (CH_4) after thaw.

68   In addition to the quantity of OM, its decomposability will influence how fast the OC in Yedoma

69 deposits can be transformed into CO_2 or CH_4 (Knoblauch et al., 2018; MacDougall and Knutti, 2016).

70 Since plants are the main source of OM in soils, vegetation composition plays an important role for OM

71 decomposability (Iversen et al., 2015). Furthermore, OM has undergone different degradation processes

72 before being incorporated into permafrost depending on permafrost formation pathways (Harden et al.,

73 2012; Waldrop et al., 2010). In epigenetic permafrost, that is permafrost aggradation through intermittent

74 freezing after the material was deposited, OM has already undergone some level of transformation and

75 easily decomposable, labile OC compounds are decomposed and lost to the atmosphere prior to

76 incorporation into the permafrost (Hugelius et al., 2012). In contrast, OM in syngenetically frozen

77 Yedoma, i.e. concurrent material deposition and permafrost aggregation, had little time to be transformed

78 prior to freezing and may thus contain high amounts of labile OM, which may be quickly decomposed to

79 greenhouse gases after thaw (Dutta et al., 2006). In this case, the amount and decomposability of the

80 fossil OM is controlled by the OM source, i.e. predominantly vegetation, which in turn depends on paleo-

81 climatic conditions (Andreev et al., 2011).

82   The decomposability of permafrost OM is often assessed based on OM degradation proxies, total OC

83 (TOC) content, total organic carbon to- total nitrogen ratios (C/N), or stable carbon isotopes ($\delta^{13}C_{org}$) with

84 contradictory results (Strauss et al., 2015; Weiss et al., 2016). Only few studies have measured CO_2 and

85 CH_4 production potentials from Siberian Yedoma deposits under laboratory conditions (Dutta et al., 2006;

86 Knoblauch et al., 2013, 2018; Lee et al., 2012; Zimov et al., 2006). In this study, we present incubation

87 data from late Pleistocene Yedoma and Holocene interglacial deposits from three locations in northeast

88 Siberia. We hypothesize that OM deposited during glacial periods experienced little pre-freezing

89 transformation and thus provides a more suitable substrate for future microbial decomposition and

90 greenhouse gas production post-thawing than Holocene deposits.

91

Biogeosciences
Open Access
EGU
Discussions

2   Study region and sample material

Three locations in the Laptev Sea region in northeast Siberia were studied (Fig. 1). The whole region is underlain by continuous permafrost reaching depths of 450–700 m onshore and 200–600 m offshore (Romanovskii et al., 2004) with ground temperatures of -11 °C for terrestrial permafrost (Drozdov et al., 2005) and -1 °C for submarine permafrost (Overduin et al., 2015). Long, cold winters and short, cool summers characterize the modern climate. Mean annual (1971–2000) temperatures and precipitation sums are -13.3 °C and 266 mm at the central Laptev Sea coast (Tiksi, WMO station 21824) and -14.9 °C and 145 mm in the eastern Laptev Sea region (Mys Shalaurova, WMO station 21647, Bulygina and Razuvaev, 2012). Modern vegetation cover is dominated by erect dwarf-shrub and in places by sedge, moss, low-shrub wetland vegetation or tussock-sedge, dwarf-shrub, moss tundra vegetation (CAVM Team, 2003). A compilation of the regional stratigraphic scheme used in this work with paleoclimate and vegetation history is summarized in Table 1.

The first study location is on Muostakh Island (71.61° N, 129.96° E), an island in the Buor Khaya Bay 40 km east of Tiksi. Between 1951–2013, the area and volume of Muostakh Island, which is subject to major coastal erosion (up to -17 m a^{-1}) and thaw subsidence, decreased by 24% and 40%, respectively (Günther et al., 2015). The entire sedimentary sequence of Muostakh Island (sample code MUO12) was sampled in three vertical sub-profiles on the northeastern shore (Meyer et al., 2015). In the current study, we used 14 sediment samples from the entire MUO12 sequence between 0.5–15.6 meters below surface (mbs), which corresponds to 19.5–4.4 meters above sea level (masl).

The second study location is on the Buor Khaya Peninsula (71.42° N, 132.11° E). Thermokarst processes affect 85% of the region, which resulted in >20 m of permafrost subsidence in some areas (Günther et al., 2013). Long-term (1969–2010) coastal erosion rates along the western coast of the Buor Khaya Peninsula are ~-1 m a^{-1} (Günther et al., 2013). On top of the Yedoma hill, approximately 100 m from the cliff edge, a 19.8 m long permafrost core (sample code BK8) was drilled (Grigoriev et al., 2013). Detailed cryolithological, geochemical, and geochronological data (Schirrmeister et al., 2017), palynological analysis (Zimmermann et al., 2017b), and lipid biomarker studies (Stapel et al., 2016) were previously published for the BK8 site. In the current study, 20 sediment samples spread evenly between the surface and 19.8 mbs (or 34 to 14.2 masl) were analyzed, excluding an ice wedge between 3.2–8.5 mbs.

The third sampling location is on Bol'shoy Lyakhovsky Island (73.34° N; 141.33° E), the southernmost island of the New Siberian Archipelago. Four cores (sample code L14) were drilled on the southern coast

Biogeosciences
Discussions

Open Access

EGU

123 (Schwamborn and Schirrmeister, 2015). Core descriptions as well as pollen and plant DNA analyses can

124 be found in Zimmermann et al. (2017a), while biomarkers and pore water analysis can be found in Stapel

125 et al. (2018). Based on previous stratigraphic studies from this location (e.g. Andreev et al., 2009;

126 Wetterich et al., 2009, 2014) we focused on two cores, which represent the here investigated MIS 1–

127 MIS 3 period. The first core, L14-05, was recovered from inside a thermokarst basin, 4 km west of the

128 Zimov'e River mouth, with Holocene thermokarst deposits overlying thawed and refrozen taberal

129 Yedoma deposits (Wetterich et al., 2009). Five sediment samples between 0–7.9 mbs (11.5–3.6 masl)

130 were analyzed for the current study. The second core, L14-02, was taken on a Yedoma hill about 1 km

131 west of the Zimov'e River mouth. The entire core was 20.0 m long, including wedge ice below 10.9 mbs.

132 Five sediment samples from the top to a depth of 10.9 mbs (32.2–21.3 masl) were incubated for the

133 current study.

134

3   Methods

3.1.   Dating

137 Radiocarbon dating was performed on plant macro fossils for MUO12 (Meyer et al., unpublished data),

138 BK8 (Schirrmeister et al., 2017), and L14 samples (Zimmermann et al., 2017a) using the AMS facilities

139 of University of Poznan and Cologne University. Additionally, feldspars grains from the BK8 core at 12.6–

140 12.75 mbs, 16.0–16.35 mbs 18.5–18.7 mbs were dated by infrared-stimulated luminescence (IRSL)

141 (Schirrmeister et al., 2017).

142

3.2.   Geochemical characteristics

144 Gravimetric water contents were calculated as the weight difference between wet and dried (105 °C)

145 samples. pH values were measured in a suspension of 5 g thawed sediment in 12.5 ml distilled water

146 (CG820, Schott AG, Mainz, Germany). For sediment chemical analyses, bulk samples were dried at

147 70°C and milled. Total carbon (TC) and total nitrogen (TN) contents were measured with an element

148 analyzer (VarioMAX cube, Elementar Analysensysteme GmbH, Hanau, Germany), while TOC contents

149 were measured with a liquiTOC II coupled to a solids module (Elementar Analysensysteme GmbH,

150 Hanau, Germany). The $\delta^{13}C_{org}$-values were measured with an isotope-ratio mass spectrometer (Delta V,

151 Thermo Scientific, Dreieich, Germany) coupled to an elemental analyzer (Flash 2000, Thermo Scientific,

152 Dreieich, Germany) after samples were treated with phosphoric acid to release inorganic carbon.

153

3.3. Incubation

Frozen samples were slowly thawed from -18 °C to 4 °C over 48 h in a refrigerator and homogenized. Anaerobic incubations were prepared under a nitrogen atmosphere in a glove box. Approximately 15–30 g thawed sediment was weighed into glass bottles and sealed with rubber stoppers. Anaerobic samples were saturated with 5–20 ml of nitrogen-flushed, CO_2-free distilled water and the headspace was exchanged with molecular nitrogen. The headspace of aerobic incubation bottles was exchanged with synthetic air (20% oxygen, 80% nitrogen).

Samples from all three study locations were incubated for 134 incubations days at 4 °C. During this time the headspace CO_2 and CH_4 concentrations were measured weekly to biweekly. The incubation of samples from the Buor Khaya Peninsula and Bol'shoy Lyakhovsky Island continued until 785 days. The measuring intervals gradually decreased to every 8–12 weeks for the remaining incubation period. Gas concentrations inside each bottle were determined by a gas chromatograph (GC 7890 Agilent Technologies, Santa Clara, USA) equipped with a nickel catalyst to reduce CO_2 to CH_4 and a flame ionizing detector (FID). Gases were separated on a PorapakQ column with helium as carrier gas. If the headspace concentration of CO_2 in aerobic incubation bottles approached 3%, the headspace was again exchanged with synthetic air.

The amount of gas in the headspace was calculated from the concentration in the headspace, headspace volume, incubation temperature, and pressure inside the bottle using the ideal gas law. The amount of gas dissolved in water was calculated from the gas concentration in the headspace, pressure inside the bottle, water content, pH, and gas solubility. Solubility for CO_2 and CH_4 in water was calculated after Carroll et al. (1991) and Yamamoto et al. (1976), respectively. To account for the dissociation of carbonic acid in water at different pH values, we used dissociation constants from Millero et al. (2007).

3.4. Statistics

Differences in mean values were analyzed with the Kruskal-Wallis test followed by multiple post-hoc Mann-Whitney tests with Bonferroni adjustment for multiple group comparisons. We tested for differences between deposits from different periods as well as for differences between deposits from the same period but from different locations. In both cases, the number of post-hoc comparisons was three, giving an adjusted significance level of 0.017. All statistical analyses were performed using MATLAB® (MATLAB and Statistics Toolbox Release 2015b, The MathWorks Inc., Natick, MA, USA).

4 Results

4.1. Chronostratigraphy and geochemical characteristics

The sedimentary sequence on Muostakh Island was divided into three sections, which were separated by two erosional contacts and sharply intersecting ice wedges (Meyer et al., 2015). Based on radiocarbon ages (Meyer et al., unpublished data), these sections could be separated into three periods. Deposits from the uppermost section between 0.5–2.4 mbs were classified as Holocene deposits from the MIS 1 and deposits from the late glacial to early Holocene transition, confirmed by radiocarbon ages of 7.5 and 13.2 ka BP for samples at 1.3 and 2.4 mbs, respectively. The middle section between 4–10 mbs yielded radiocarbon ages of 16.1–18.9 ka BP and were therefore classified as Sartan stadial deposits from the MIS 2. The lowermost section between 11.3–15.6 mbs yielded radiocarbon ages of 41.6–45.9 ka BP and represents the MIS 3 Kargin interstadial.

The BK8 core from the Buor Khaya Peninsula was subdivided into four sections. The first section between 0–0.5 mbs represents the seasonally thawed active layer. The subdivision of the permafrost deposits below the active layer was based on previously published radiocarbon and IRSL ages (Schirrmeister et al., 2017). Deposits from the second section between 0.5–3.2 mbs yielded radiocarbon ages between 9.7–11.4 ka BP, which corresponds to the late glacial transition to the early Holocene. The third section between 3.2–8.5 mbs consisted of an ice wedge, which was not sampled for the current study. The fourth section between 8.5–18.9 mbs yielded infinite radiocarbon ages of >50 ka BP. The additional IRSL ages of feldspar grains yielded deposition ages of ~45 ka BP. Thus, sediments from this section were classified as deposits from the Kargin interstadial.

The upper 0.5 m from both cores from Bol'shoy Lyakhovsky Island represent the active layer. Radiocarbon ages of the L14-05 core from the thermokarst basin ranged between 2.2–10.1 ka BP for the upper core section between 0–1.7 mbs and 51.2–54.6 ka BP for deposits below 5.8 mbs (Zimmermann et al., 2017a). Based on these ages, stratigraphic interpretations from a nearby outcrop (Wetterich et al., 2009) and the available palynological data (Zimmermann et al., 2017a), the L14-05 core was divided into two parts. The upper part between 0–5.5 mbs were deposited during the Holocene and late glacial transition, while deposits below 5.5 mbs was deposited during the Kargin interstadial. Deposits from the L14-02 core from the Yedoma hill yielded radiocarbon ages between 33.1–62.8 ka BP, which corresponds to deposition during the MIS3 Kargin interstadial.

Overall, the permafrost deposits showed a wide range in TOC contents (0.8 – 6.3 wt%), C/N (4.6 – 29.4), and $\delta^{13}C_{org}$ (-29.0 – -22.8 ‰VPDB, Fig. 2). Generally higher TOC contents and C/N were found in

216 deposits from the Holocene and Kargin interstadial than in deposits from the Sartan stadial (Mann-
217 Whitney test, $p < 0.017$), while the $\delta^{13}C_{org}$-values were significantly higher in Sartan stadial deposits
218 (Mann-Whitney test, $p < 0.001$).

219

220 4.2. Muostakh Island

221 Based on the TOC content, CO_2 production after 134 incubation days from sediment samples from the
222 MUO12 sequence ranged between 4.8–60.7 mg CO_2-C g^{-1} OC under aerobic conditions and 0.5–20.9
223 mg CO_2-C g^{-1} OC under anaerobic conditions (Fig. 3). Higher aerobic CO_2 production was generally
224 observed in the lowermost Kargin deposits between 11.3–15.6 mbs but elevated CO_2 production rates
225 were also observed at 1.6 mbs, 6 mbs, and 10 mbs. Under anaerobic conditions, the highest production
226 was observed at 6 mbs (19.3 ± 1.4 mg CO_2-C g^{-1} OC), which was nearly twice as high as in most other
227 samples. No methanogenesis was observed in any Muostakh Island samples over the 134-day
228 incubation period.

229

230 4.3. Buor Khaya Peninsula

231 After 134 incubation days, CO_2 production in BK8 core samples ranged between 2.2–64.1 mg CO_2-C g^{-1}
232 OC aerobically and 2.2–17.1 mg CO_2-C g^{-1} OC anaerobically (Fig. 4), which is within the same range as
233 production in samples from Muostakh Island over the same incubation period (Fig. 3). The highest
234 production was observed in the active layer. Production then decreased sharply between 0.5–3.2 mbs
235 but increased again in Kargin interstadial deposits below the ice-wedge. Methanogenesis was only
236 observed in the active layer, but in much smaller quantity than anaerobic CO_2 (0.37 ± 0.22 mg CH_4-C g^{-1}
237 OC compared to 13.3 ± 3.6 mg CO_2-C g^{-1} OC).

238 To assess the long-term decomposability, all BK8 core samples were incubated for a total of 785
239 days. After 785 incubation days, CO_2 production ranged between 4.6–131.1 mg CO_2-C g^{-1} OC under
240 aerobic conditions and 2.2–43.0 mg CO_2-C g^{-1} OC under anaerobic conditions. CO_2 production rates,
241 however, decreased sharply within the first weeks of incubation. On average, 58 ± 12% of the aerobically
242 and 86 ± 24% of the anaerobically produced CO_2 after 785 incubation days was already produced within
243 the first 134 days. In contrast, CH_4 production in the active layer increased 30-fold to 11.4 ± 3.0 mg
244 CH_4-C g^{-1} OC. Additionally, two out of three replicates at 10 mbs also showed active methanogenesis
245 after 785 days (4.0 mg CH_4-C g^{-1} OC and 12.7 mg CH_4-C g^{-1} OC, respectively).

246

4.4. Bol'shoy Lyakhovsky Island

Aerobic CO_2 production after 134 incubation days in samples from the L14 cores ranged between 3.7–18.9 mg CO_2-C g^{-1} OC (Fig. Figure **5**). The mean aerobic CO_2 production in all Kargin interstadial deposits from Bol'shoy Lyakhovsky Island (9.2 ± 4.7 mg CO_2-C g^{-1} OC) was significantly lower (Mann-Whitney test, p < 0.001) than CO_2 production in MIS 3 deposits from Muostakh Island (32.2 ± 15.6 mg CO_2-C g^{-1} OC) and the Buor Khaya Peninsula (26.0 ± 12.6 mg CO_2-C g^{-1} OC). Anaerobic CO_2 production in Kargin deposits ranged between 3.2–11.6 mg CO_2-C g^{-1} OC, which was within the same range as production observed from the other two locations. No CH_4 production was observed in any L14 samples after 134 days.

After 785 incubation days, aerobic and anaerobic CO_2 production ranged between 11.0–55.2 mg CO_2-C g^{-1} OC and 3.0–27.0 mg CO_2-C g^{-1} OC, respectively. Active methanogenesis was only observed in 2 out of 3 replicates from the active layer from the L14-05 core (0.41 mg CH_4-C g^{-1} OC and 0.63 mg CH_4-C g^{-1} OC). CH_4 production was therefore an order of magnitude lower than anaerobic CO_2 production in the same sample (5.7 mg CO_2-C g^{-1} OC and 4.6 mg CO_2-C g^{-1} OC) and also an order of magnitude smaller than CH_4 production in the active layer from the Buor Khaya Peninsula.

4.5. Decomposability of permafrost OM deposited under different climatic regimes

Overall, permafrost OM deposited during the MIS 3 Kargin interstadial supported the highest greenhouse gas production (Fig. Figure **6**). After 134 days of aerobic incubation, 0.2–6.1% of the initially available OC (mean 2.3 ± 1.4%) was decomposed to CO_2. This was significantly more (Mann-Whitney test, p < 0.001) than in deposits from the Holocene and late glacial transition, where production ranged between 0.4–4.0% (mean 1.2 ± 0.8%). The aerobic CO_2 production in MIS 2 Sartan stadial deposits ranged between 0.5–4.2% (mean 1.7 ± 1.2 %). Anaerobically, 3.3 times less CO_2 was produced (Pearson correlation coefficient r = 0.63, p < 0.001). The lowest production was observed in Holocene and late glacial transition deposits, where 0.1–1.1 % of the OC was anaerobically decomposed to CO_2 (mean 0.5 ± 0.3). This was significantly less (Mann-Whitney test, p < 0.01) than in glacial deposits, where 0.4–2.1% (mean 0.9 ± 0.5%) and 0.2–1.6 % of initial OC (mean 0.7 ± 0.3%) were decomposed in Sartan stadial and Kargin interstadial deposits, respectively.

5   Discussion

5.1. Organic matter decomposability

The ice-rich permafrost deposits of Muostakh Island, the Buor Khaya Peninsula, and Bol'shoy Lyakhovsky Island are typical for northeast Siberia and the geochemical characteristics (TOC, C/N, $\delta^{13}C_{org}$) were all within the range of other permafrost deposits in the region (Schirrmeister et al., 2011). We hypothesized, that the climatic conditions during deposition affected the amount and decomposability of preserved OM and thus greenhouse gas production potentials after thaw. OM decomposability in degrading ice-rich permafrost therefore needs to be interpreted against the paleo-environmental background.

One way to analyze the OM source in more detail is sedimentary ancient DNA (sedaDNA), which can be used to reconstruct local plant communities and infer predominant climatic conditions (Willerslev et al., 2004). In the BK8 core, a total of 134 vascular plants and 20 bryophytes were identified (Zimmermann et al., 2017b). *Salix*, Poaceae and Cyperaceae, whose roots are a main OM source in tundra soils (Iversen et al., 2015), are present throughout the core. The taxonomic richness was highest between 8.35–16 mbs, where also high CO_2 production was observed. This core section, which belongs to the MIS 3 Kargin interstadial (Schirrmeister et al., 2017), was dominated by swamp and aquatic taxa, pointing towards a water-saturated environment, likely a low-centered ice-wedge polygon (Zimmermann et al., 2017b). Together with higher TOC contents at these depths, this suggests accumulation of relatively undecomposed OM under anaerobic conditions, which can be quickly decomposed after thaw (de Klerk et al., 2011). Furthermore, high concentrations of branched glycerol dialkyl glycerol tetraether (br-GDGT), a microbial membrane compound, are indicative of a soil microbial community, which developed when the climate was relatively warm and wet (Stapel et al., 2016). Overall, br-GDGT concentrations were highest at 10 mbs, 11.2 mbs, and 15 mbs (Stapel et al., 2016), which corresponds to the same levels where the highest CO_2 production was observed. In contrast, lower abundance of swamp taxa and higher abundance of terrestrial taxa at 8.8 mbs and >15 mbs (Zimmermann et al., 2017b), suggest that intermittently drier conditions existed. This resulted in accelerated OM decomposition under aerobic conditions prior to OM incorporation into the permafrost, lower TOC contents as well as lower CO_2 production potentials at these depths.

Sediments above the ice-wedge in the BK8 core showed similar TOC contents, C/N, and $\delta^{13}C_{org}$-values compared to the rest of the core, but CO_2 production was consistently low in this section. This ~3 m long core section yielded radiocarbon ages of 11.4–10.1 ka BP (Schirrmeister et al., 2017), which

corresponds to the late glacial-early Holocene transition. After the Last Glacial Maximum (LGM), temperatures were favorable for increased microbial decomposition of active layer OM, which led to the preservation of comparatively stable OM fractions after the material was incorporated into the permafrost. Similar conclusions can be drawn for Holocene deposits in thermokarst landforms or on top of Yedoma deposits. On the one hand, they received fresh OM inputs, which explains their relatively high TOC contents (Strauss et al., 2015). On the other hand, intensive thermokarst development during the late glacial transition and the early Holocene likely resulted in higher decomposition rates in thawed soils and the loss of labile OM compounds before the sediments were refrozen when climate conditions deteriorated after the Holocene climate optimum. If these sediments were to thaw again in the future, results from the current study suggest that the decomposability of the remaining OM will be comparatively low. Although climatic conditions influence the vegetation composition and OM source on a regional level, the local depositional environment as well as post-depositional processes likely also control the amount and decomposability of the OM that is presently incorporated into permafrost.

First results of *in situ* CO_2 fluxes from Muostakh Island were published by Vonk et al. (2012). They estimate that 66% of the thawed out OC from degrading ice-rich permafrost deposits can be decomposed to greenhouse gases and released back to the atmosphere before the material is reburied in the Laptev Sea. However, no further detailed palynological or microbial biomarker studies are yet available for the MUO12 sequence. The closest reference locations is the comprehensive permafrost record at the Mamontovy Khayata section on the Bykovsky Peninsula (Andreev et al., 2002; Sher et al., 2005). Sea level rise after the last glacial period, coastal erosion, and marine ingression of thermokarst basins eventually separated Muostakh Island from the Bykovsky Peninsula (Grosse et al., 2007; Romanovskii et al., 2004). Today, the distance between the northern tip of Muostakh Island and the southern tip of the Bykovsky Peninsula is about 16 km. Between 58–12 ka BP (Schirrmeister et al., 2002), fine-grained material accumulated on the large flat foreland plain of the today Bykovsky Peninsula area that was exposed at a time of lower sea level (Grosse et al., 2007). The distance between Muostakh Island and the Buor Khaya Peninsula is about 80 km. It is therefore likely that the deposition regimes on Muostakh Island and the Buor Khaya Peninsula were similar to the regime at the Bykovsky Peninsula. This conclusion is also supported by similar OM decomposability. After 134 incubation days, the amount of CO_2 production did not differ significantly (Mann-Whitney test, $p = 0.339$) between MIS 3 Kargin deposits from Muostakh Island (3.2 ± 1.6% of initial OC aerobically and 0.7 ± 0.6% anaerobically) and the BK8

337 core (2.7 ± 1.2% aerobically and 0.8 ± 0.3 % anaerobically), which suggests that the deposits formed
338 under similar conditions.

339   Under aerobic conditions, CO_2 production of MIS 3 deposits from Bol'shoy Lyakhovsky Island in the
340 eastern Laptev Sea was nearly three times lower (0.9 ± 0.5% of the initial OC after 134 days) than
341 observed for Muostakh Island and the Buor Khaya Peninsula in the central Laptev Sea. Considerably
342 lower temperatures and precipitation characterize the modern climate on Bol'shoy Lyakhovsky Island. It
343 is also likely that regional differences between the eastern and central Laptev Sea region would have
344 affected the paleo-climate (Anderson and Lozhkin, 2001; Lozhkin and Anderson, 2011; Wetterich et al.,
345 2011, 2014). Different summer temperatures, precipitation, thaw depth, and vegetation composition
346 could explain regional differences in OM quantity and decomposability. Interestingly, the differences in
347 the amount of OC that was aerobically decomposed were mostly due to differences in the initial CO_2
348 production rates. Maximum CO_2 production rates during the first weeks of incubation of Muostakh Island
349 and Buor Khaya deposits were up to four times higher than in deposits from Bol'shoy Lyakhovsky Island.
350 However, long-term production rates after >130 incubation days did no longer differ considerably
351 between the different locations (median 23.3 µg CO_2-C g^{-1} OC d^{-1}). These rates are within the range of
352 other long-term production rates from Yedoma deposits in northeast Siberia (Dutta et al., 2006;
353 Knoblauch et al., 2013) and Alaska (Lee et al., 2012). Considering the large slowly decomposing
354 permafrost OC pool (Schädel et al., 2014), long-term decomposition rates are likely to provide more
355 reliable projections of future greenhouse gas emissions from degrading permafrost landscapes.

356   A distinctive feature of the Muostakh Island sequence is the preservation of MIS 2 Sartan deposits,
357 which are only sparsely preserved in northeast Siberia (Wetterich et al., 2011). Interestingly, mean
358 aerobic CO_2 production in Sartan deposits from Muostakh Island was lower than in Kargin deposits, but
359 slightly higher under anaerobic conditions, but the difference was not statistically significant (Mann-
360 Whitney test, $p = 0.205$). The rapid deposition of 8 m thick comparatively coarse-grained material in just
361 a few thousand years between 20–16 ka BP were unfavorable for the development of a stable land
362 surface and the establishment of a vegetation cover comparable to the Kargin interstadial or Holocene
363 periods (Meyer et al., unpublished data). Pollen analysis from the corresponding sections on the
364 Bykovsky Peninsula (Andreev et al., 2002) and Kurungnakh Island in the Lena River Delta (Schirrmeister
365 et al., 2008; Wetterich et al., 2008) suggest relatively cold and dry summer conditions during this stadial
366 with sparse vegetation. Relatively undecomposed OM was quickly buried, before it could be transformed
367 to greenhouse gases.

368

5.2. Long-term production potentials

Long-term greenhouse gas production measurements after 785 days showed that 51% of the aerobically and 83% of the anaerobically produced CO_2 were already produced within the first 134 incubation days, highlighting the non-linearity of OM decomposition dynamics (Knoblauch et al., 2013; Schädel et al., 2014) and the importance of the labile OC pool in short term incubations. Assuming no new input of labile OM (e.g. from modern vegetation), decomposition rates are likely to remain low after the labile pool is depleted. Short-term greenhouse gas production and release from thawing ice-rich permafrost will therefore mainly depend on the size of the labile pool. A synthesis study of several incubations studies from high-latitude soils, including Yedoma deposits, estimated the size of the labile OC pool to be generally <5% of the TOC (Schädel et al., 2014). For Yedoma deposits on nearby Kurungnakh Island in the Lena River delta, Knoblauch et al. (2013) estimated the size of the labile pool to be even smaller (<2%).

5.3. Methanogenesis

CH_4 production from Yedoma deposits, or the lack thereof, is a highly controversial topic in permafrost research (Knoblauch et al., 2018; Rivkina et al., 1998; Treat et al., 2015). In the current work, active methanogenesis was only observed in the active layer and 2 out of 38 Yedoma samples from the BK8 core, but only after a long lag-phase. Within 134 incubation days, no samples from Muostakh Island produced any CH_4. . In those samples showing active methanogenesis, CH_4 production continued to rise over the 785 incubation days, which is in contrast to anaerobic CO_2 production, which decreased with increasing incubation time. Rising CH_4 production rates indicate that methanogenic communities still grow in these samples and were not limited by substrate supply. Chemical pore water and bulk sediment analyses from the BK8 core showed that there are high concentrations of both free and OM-bound acetate present in Yedoma deposits, indicating a high substrate potential for methanogenesis (Stapel et al., 2016). Knoblauch et al. (2018) showed that the small contribution of methanogenesis to overall anaerobic permafrost OM decomposition found in short-term incubation studies (Treat et al., 2015) is due to the absence of an active methanogenic community. On a multi-annual timescale, methanogenic communities become active and equal amounts of CO_2 and CH_4 are produced from permafrost OM under anaerobic conditions. Under future climate warming and renewed thermokarst activity, high levels of CH_4 production can locally be expected but depend on favorable conditions such as above-zero

399 temperatures and anaerobic conditions. It can be expected that the development of an active
400 methanogenic community e.g. by growth or downward migration of modern methanogenic organisms
401 will lead to elevated long-term CH_4 production in these deposits (Knoblauch et al., 2018).
402

6   Conclusion

404 In this study, we investigated greenhouse gas production potentials in degrading ice-rich permafrost
405 deposits from three locations in northeast Siberia. It could be shown that Yedoma deposits generally
406 contained more labile OM than Holocene deposits. However, in addition to the regional climate conditions
407 at the time of OM deposition, local depositional environments also influenced the amount and
408 decomposability of the preserved fossil OM. Within the deposits of the MIS 3 Kargin interstadial,
409 sediments deposited under wet and possibly anaerobic conditions produced more CO_2 than sediments
410 deposited under drier aerobic conditions. It is therefore likely, that OM decomposability of the vast
411 Yedoma landscape cannot be generalized solely based on the stratigraphic position. Furthermore, it is
412 expected that CH_4 production will play a more prominent role after active methanogenic communities
413 have established since abundant substrates for methanogenesis were present.
414

Data availability

416 https://www.pangaea.de/ (follows after acceptance and includes all shown datasets)
417

Author contributions

419 JW and CK designed the study. TO collected sediment samples on Muostakh Island and LS collected
420 cores from the Buor Khaya Peninsula and Bol'shoy Lyakhovsky Island. JW and RT performed the
421 laboratory analyses, with guidance from CK and EMP. JW performed data analyses and wrote the
422 manuscript with contributions from all authors.
423

Acknowledgements

Biogeosciences
Discussions

Open Access

EGU

434

435 **References**

436 Anderson, P. M. and Lozhkin, A. V.: The Stage 3 interstadial complex (Karginskii/middle Wisconsinan
437 interval) of Beringia: variations in paleoenvironments and implications for paleoclimatic interpretations,
438 Quat. Sci. Rev., 20(1–3), 93–125, doi:10.1016/S0277-3791(00)00129-3, 2001.

439 Andreev, A. A., Schirrmeister, L., Siegert, C., Bobrov, A. A., Demske, D., Seiffert, M. and Hubberten, H.-
440 W.: Paleoenvironmental changes in northeastern Siberia during the Late Quaternary - Evidence from
441 pollen records of the Bykovsky Peninsula, Polarforschung, 70, 13–25, 2002.

442 Andreev, A. A., Grosse, G., Schirrmeister, L., Kuznetsova, T. V., Kuzmina, S. A., Bobrov, A. A., Tarasov,
443 P. E., Novenko, E. Y., Meyer, H., Derevyagin, A. Y., Kienast, F., Bryantseva, A. and Kunitsky, V. V.:
444 Weichselian and Holocene palaeoenvironmental history of the Bol'shoy Lyakhovsky Island, New
445 Siberian Archipelago, Arctic Siberia, Boreas, 38(1), 72–110, doi:10.1111/j.1502-3885.2008.00039.x,
446 2009.

447 Andreev, A. A., Schirrmeister, L., Tarasov, P. E., Ganopolski, A., Brovkin, V., Siegert, C., Wetterich, S.
448 and Hubberten, H.-W.: Vegetation and climate history in the Laptev Sea region (Arctic Siberia) during
449 Late Quaternary inferred from pollen records, Quat. Sci. Rev., 30(17–18), 2182–2199,
450 doi:10.1016/j.quascirev.2010.12.026, 2011.

451 Brown, J., Ferrians Jr, O. J., Heginbottom, J. A. and Melnikov, E. S.: Circum-Arctic map of permafrost
452 and ground-ice conditions. Boulder, CO: National Snow and Ice Data Center/World Data Center for
453 Glaciology, Digit. media, 1998.

454 Bulygina, O. N. and Razuvaev, V. N.: Daily temperature and precipitation data for 518 Russian
455 meteorological stations, Carbon Dioxide Information Analysis Center, Oak Ridge National Laboratory,
456 U.S. Department of Energy, Oak Ridge, Tennessee (USA), 2012.

457 Carroll, J. J., Slupsky, J. D. and Mather, A. E.: The solubility of carbon dioxide in water at low pressure,
458 J. Phys. Chem. Ref. Data, 20(6), 1201, doi:10.1063/1.555900, 1991.

459 CAVM Team: Circumpolar Arctic Vegetation Map (1:7,500,000 scale), Conservation of Arctic Flora and
460 Fauna (CAFF) Map No. 1, U.S. Fish and Wildlife Service, Anchorage, Alaska, 2003.

461 Drozdov, D. S., Rivkin, F. M., Rachold, V., Ananjeva-Malkova, G. V., Ivanova, N. V., Chehina, I. V.,
462 Koreisha, M. M., Korostelev, Y. V. and Melnikov, E. S.: Electronic atlas of the Russian Arctic coastal
463 zone, Geo-Marine Lett., 25(2–3), 81–88, doi:10.1007/s00367-004-0189-7, 2005.

464 Dutta, K., Schuur, E. A. G., Neff, J. C. and Zimov, S. A.: Potential carbon release from permafrost soils
465 of Northeastern Siberia, Glob. Chang. Biol., 12(12), 2336–2351, doi:10.1111/j.1365-2486.2006.01259.x,
466 2006.

467 van Everdingen, R.: Multi-language glossary of permafrost and related ground-ice terms, [online]

15

468   Available from: http://nsidc.org/fgdc/glossary/ (Accessed 1 January 2015), 2005.

469   Grigoriev, M. N., Overduin, P. P., Schirrmeister, L. and Wetterich, S.: Scientific permafrost drilling
470   campaign, in Russian-German cooperation SYSTEM LAPTEV SEA : The Expeditions Laptev Sea -
471   Mamontov Klyk 2011 & Buor Khaya 2012, vol. 664, edited by F. Günther, P. P. Overduin, A. S. Makarov,
472   and M. N. Grigoriev, pp. 75–86, Reports on Polar and Marine Research, 2013.

473   Grosse, G., Schirrmeister, L., Siegert, C., Kunitsky, V. V., Slagoda, E. A., Andreev, A. A. and Dereviagyn,
474   A. Y.: Geological and geomorphological evolution of a sedimentary periglacial landscape in Northeast
475   Siberia during the Late Quaternary, Geomorphology, 86(1–2), 25–51,
476   doi:10.1016/j.geomorph.2006.08.005, 2007.

477   Grosse, G., Robinson, J. E., Bryant, R., Taylor, M. D., Harper, W., DeMasi, A., Kyker-Snowman, E.,
478   Veremeeva, A., Schirrmeister, L. and Harden, J.: Distribution of late Pleistocene ice-rich syngenetic
479   permafrost of the Yedoma Suite in east and central Siberia, Russia. [online] Available from:
480   http://epic.awi.de/33878/, 2013.

481   Günther, F., Overduin, P. P., Sandakov, a. V., Grosse, G. and Grigoriev, M. N.: Short- and long-term
482   thermo-erosion of ice-rich permafrost coasts in the Laptev Sea region, Biogeosciences, 10(6), 4297–
483   4318, doi:10.5194/bg-10-4297-2013, 2013.

484   Günther, F., Overduin, P. P., Yakshina, I. A., Opel, T., Baranskaya, A. V. and Grigoriev, M. N.: Observing
485   Muostakh disappear: Permafrost thaw subsidence and erosion of a ground-ice-rich island in response
486   to arctic summer warming and sea ice reduction, Cryosph., 9(1), 151–178, doi:10.5194/tc-9-151-2015,
487   2015.

488   Harden, J. W., Koven, C. D., Ping, C.-L., Hugelius, G., David McGuire, A., Camill, P., Jorgenson, T.,
489   Kuhry, P., Michaelson, G. J., O'Donnell, J. A., Schuur, E. A. G., Tarnocai, C., Johnson, K. and Grosse,
490   G.: Field information links permafrost carbon to physical vulnerabilities of thawing, Geophys. Res. Lett.,
491   39(15), 1–6, doi:10.1029/2012GL051958, 2012.

492   Hugelius, G., Routh, J., Kuhry, P. and Crill, P.: Mapping the degree of decomposition and thaw
493   remobilization potential of soil organic matter in discontinuous permafrost terrain, J. Geophys. Res.
494   Biogeosciences, 117(G2), G02030, doi:10.1029/2011JG001873, 2012.

495   Hugelius, G., Strauss, J., Zubrzycki, S., Harden, J. W., Schuur, E. A. G., Ping, C.-L., Schirrmeister, L.,
496   Grosse, G., Michaelson, G. J., Koven, C. D., O'Donnell, J. A., Elberling, B., Mishra, U., Camill, P., Yu,
497   Z., Palmtag, J. and Kuhry, P.: Estimated stocks of circumpolar permafrost carbon with quantified
498   uncertainty ranges and identified data gaps, Biogeosciences, 11(23), 6573–6593, doi:10.5194/bg-11-
499   6573-2014, 2014.

500   Iversen, C. M., Sloan, V. L., Sullivan, P. F., Euskirchen, E. S., McGuire, A. D., Norby, R. J., Walker, A.
501   P., Warren, J. M. and Wullschleger, S. D.: The unseen iceberg: Plant roots in arctic tundra, New Phytol.,
502   205(1), 34–58, doi:10.1111/nph.13003, 2015.

503   Kanevskiy, M., Shur, Y., Fortier, D., Jorgenson, M. T. and Stephani, E.: Cryostratigraphy of late
504   Pleistocene syngenetic permafrost (yedoma) in northern Alaska, Itkillik River exposure, Quat. Res.,
505   75(3), 584–596, doi:10.1016/j.yqres.2010.12.003, 2011.

506   de Klerk, P., Donner, N., Karpov, N. S., Minke, M. and Joosten, H.: Short-term dynamics of a low-centred
507   ice-wedge polygon near Chokurdakh (NE Yakutia, NE Siberia) and climate change during the last ca
508   1250 years, Quat. Sci. Rev., 30(21–22), 3013–3031, doi:10.1016/j.quascirev.2011.06.016, 2011.

Knoblauch, C., Beer, C., Sosnin, A., Wagner, D. and Pfeiffer, E.-M.: Predicting long-term carbon mineralization and trace gas production from thawing permafrost of Northeast Siberia, Glob. Chang. Biol., 19(4), 1160–1172, doi:10.1111/gcb.12116, 2013.

Knoblauch, C., Beer, C., Liebner, S., Grigoriev, M. N. and Pfeiffer, E.-M.: Methane production as key to the greenhouse gas budget of thawing permafrost, Nat. Clim. Chang., 8(4), 309–312, doi:10.1038/s41558-018-0095-z, 2018.

Lee, H., Schuur, E. A. G., Inglett, K. S., Lavoie, M. and Chanton, J. P.: The rate of permafrost carbon release under aerobic and anaerobic conditions and its potential effects on climate, Glob. Chang. Biol., 18(2), 515–527, doi:10.1111/j.1365-2486.2011.02519.x, 2012.

Lozhkin, A. V. and Anderson, P. M.: Forest or no forest: Implications of the vegetation record for climatic stability in Western Beringia during oxygen isotope stage 3, Quat. Sci. Rev., 30(17–18), 2160–2181, doi:10.1016/j.quascirev.2010.12.022, 2011.

MacDougall, A. H. and Knutti, R.: Projecting the release of carbon from permafrost soils using a perturbed parameter ensemble modelling approach, Biogeosciences, 13(7), 2123–2136, doi:10.5194/bg-13-2123-2016, 2016.

Meyer, H., Opel, T. and Dereviagin, A.: Stratigraphic and sedimentological studies, in Russian-German Cooperation SYSTEM LAPTEV SEA: The expedition Lena 2012, pp. 79–82, Reports on Polar and Marine Research, 2015.

Millero, F., Huang, F., Graham, T. and Pierrot, D.: The dissociation of carbonic acid in NaCl solutions as a function of concentration and temperature, Geochim. Cosmochim. Acta, 71(1), 46–55, doi:10.1016/j.gca.2006.08.041, 2007.

Morgenstern, A., Ulrich, M., Günther, F., Roessler, S., Fedorova, I. V., Rudaya, N. A., Wetterich, S., Boike, J. and Schirrmeister, L.: Evolution of thermokarst in East Siberian ice-rich permafrost: A case study, Geomorphology, 201, 363–379, doi:10.1016/j.geomorph.2013.07.011, 2013.

Natali, S. M., Schuur, E. A. G., Mauritz, M., Schade, J. D., Celis, G., Crummer, K. G., Johnston, C., Krapek, J., Pegoraro, E., Salmon, V. G. and Webb, E. E.: Permafrost thaw and soil moisture driving CO_2 and CH_4 release from upland tundra, J. Geophys. Res. Biogeosciences, 120(3), 525–537, doi:10.1002/2014JG002872, 2015.

Opel, T., Wetterich, S., Meyer, H., Dereviagin, A. Y., Fuchs, M. C. and Schirrmeister, L.: Ground-ice stable isotopes and cryostratigraphy reflect late Quaternary palaeoclimate in the Northeast Siberian Arctic (Oyogos Yar coast, Dmitry Laptev Strait), Clim. Past, 13(6), 587–611, doi:10.5194/cp-13-587-2017, 2017.

Overduin, P. P., Liebner, S., Knoblauch, C., Günther, F., Wetterich, S., Schirrmeister, L., Hubberten, H.-W. and Grigoriev, M. N.: Methane oxidation following submarine permafrost degradation: Measurements from a central Laptev Sea shelf borehole, J. Geophys. Res. Biogeosciences, 120, 1–14, doi:10.1002/2014JG002862.Received, 2015.

Ping, C. L., Jastrow, J. D., Jorgenson, M. T., Michaelson, G. J. and Shur, Y. L.: Permafrost soils and carbon cycling, SOIL, 1(1), 147–171, doi:10.5194/soil-1-147-2015, 2015.

Rivkina, E., Gilichinsky, D., Wagener, S., Tiedje, J. and McGrath, J.: Biogeochemical activity of anaerobic microorganisms from buried permafrost sediments, Geomicrobiol. J., 15(3), 187–193,

549   doi:10.1080/01490459809378075, 1998.

550   Romanovskii, N. N., Hubberten, H.-W., Gavrilov, A. V., Tumskoy, V. E. and Kholodov, A. L.: Permafrost
551   of the east Siberian Arctic shelf and coastal lowlands, Quat. Sci. Rev., 23(11–13), 1359–1369,
552   doi:10.1016/j.quascirev.2003.12.014, 2004.

553   Schädel, C., Schuur, E. A. G., Bracho, R., Elberling, B., Knoblauch, C., Lee, H., Luo, Y., Shaver, G. R.
554   and Turetsky, M. R.: Circumpolar assessment of permafrost C quality and its vulnerability over time using
555   long-term incubation data, Glob. Chang. Biol., 20(2), 641–652, doi:10.1111/gcb.12417, 2014.

556   Schirrmeister, L., Siegert, C., Kuznetsova, T., Kuzmina, S., Andreev, A., Kienast, F., Meyer, H. and
557   Bobrov, A.: Paleoenvironmental and paleoclimatic records from permafrost deposits in the Arctic region
558   of Northern Siberia, Quat. Int., 89(1), 97–118, doi:10.1016/S1040-6182(01)00083-0, 2002.

559   Schirrmeister, L., Grosse, G., Kunitsky, V., Magens, D., Meyer, H., Dereviagin, A., Kuznetsova, T.,
560   Andreev, A., Babiy, O., Kienast, F., Grigoriev, M., Overduin, P. P. and Preusser, F.: Periglacial landscape
561   evolution and environmental changes of Arctic lowland areas for the last 60000 years (western Laptev
562   Sea coast, Cape Mamontov Klyk), Polar Res., 27(2), 249–272, doi:10.1111/j.1751-8369.2008.00067.x,
563   2008.

564   Schirrmeister, L., Kunitsky, V., Grosse, G., Wetterich, S., Meyer, H., Schwamborn, G., Babiy, O.,
565   Derevyagin, A. and Siegert, C.: Sedimentary characteristics and origin of the Late Pleistocene Ice
566   Complex on north-east Siberian Arctic coastal lowlands and islands – A review, Quat. Int., 241(1–2), 3–
567   25, doi:10.1016/j.quaint.2010.04.004, 2011.

568   Schirrmeister, L., Froese, D., Tumskoy, V., Grosse, G. and Wetterich, S.: Yedoma: Late Pleistocene ice-
569   rich syngenetic permafrost of Beringia, in Encyclopedia of Quaternary Science, edited by S. A. Elias, pp.
570   542–552, Elsevier, Amsterdam, doi:10.1016/B978-0-444-53643-3.00106-0, 2013.

571   Schirrmeister, L., Schwamborn, G., Overduin, P. P., Strauss, J., Fuchs, M. C., Grigoriev, M., Yakshina,
572   I., Rethemeyer, J., Dietze, E. and Wetterich, S.: Yedoma Ice Complex of the Buor Khaya Peninsula
573   (southern Laptev Sea), Biogeosciences, 14(5), 1261–1283, doi:10.5194/bg-14-1261-2017, 2017.

574   Schneider von Deimling, T., Meinshausen, M., Levermann, A., Huber, V., Frieler, K., Lawrence, D. M.
575   and Brovkin, V.: Estimating the near-surface permafrost-carbon feedback on global warming,
576   Biogeosciences, 9(2), 649–665, doi:10.5194/bg-9-649-2012, 2012.

577   Schneider von Deimling, T., Grosse, G., Strauss, J., Schirrmeister, L., Morgenstern, A., Schaphoff, S.,
578   Meinshausen, M. and Boike, J.: Observation-based modelling of permafrost carbon fluxes with
579   accounting for deep carbon deposits and thermokarst activity, Biogeosciences, 12(11), 3469–3488,
580   doi:10.5194/bg-12-3469-2015, 2015.

581   Schuur, E. A. G., McGuire, A. D., Schädel, C., Grosse, G., Harden, J. W., Hayes, D. J., Hugelius, G.,
582   Koven, C. D., Kuhry, P., Lawrence, D. M., Natali, S. M., Olefeldt, D., Romanovsky, V. E., Schaefer, K.,
583   Turetsky, M. R., Treat, C. C. and Vonk, J. E.: Climate change and the permafrost carbon feedback,
584   Nature, 520(7546), 171–179, doi:10.1038/nature14338, 2015.

585   Schwamborn, G. and Schirrmeister, L.: Permafrost drilling on Bol'shoy Lyakhovsky, in Russian-German
586   Cooperation CARBOPERM: Field campaigns to Bol'shoy Lyakhovsky Island in 2014, pp. 11–19., 2015.

587   Sher, A. V., Kuzmina, S. A., Kuznetsova, T. V. and Sulerzhitsky, L. D.: New insights into the Weichselian
588   environment and climate of the East Siberian Arctic, derived from fossil insects, plants, and mammals,

589 Quat. Sci. Rev., 24(5–6), 533–569, doi:10.1016/j.quascirev.2004.09.007, 2005.

590 Stapel, J. G., Schirrmeister, L., Overduin, P. P., Wetterich, S., Strauss, J., Horsfield, B. and Mangelsdorf,
591 K.: Microbial lipid signatures and substrate potential of organic matter in permafrost deposits:
592 Implications for future greenhouse gas production, J. Geophys. Res. Biogeosciences, 121(10), 2652–
593 2666, doi:10.1002/2016JG003483, 2016.

594 Stapel, J. G., Schwamborn, G., Schirrmeister, L., Horsfield, B. and Mangelsdorf, K.: Substrate potential
595 of last interglacial to Holocene permafrost organic matter for future microbial greenhouse gas production,
596 Biogeosciences, 15(7), 1969–1985, doi:10.5194/bg-15-1969-2018, 2018.

597 Strauss, J., Schirrmeister, L., Grosse, G., Wetterich, S., Ulrich, M., Herzschuh, U. and Hubberten, H.-
598 W.: The deep permafrost carbon pool of the Yedoma region in Siberia and Alaska, Geophys. Res. Lett.,
599 40(23), 6165–6170, doi:10.1002/2013GL058088, 2013.

600 Strauss, J., Schirrmeister, L., Mangelsdorf, K., Eichhorn, L., Wetterich, S. and Herzschuh, U.: Organic-
601 matter quality of deep permafrost carbon – A study from Arctic Siberia, Biogeosciences, 12(7), 2227–
602 2245, doi:10.5194/bg-12-2227-2015, 2015.

603 Strauss, J., Schirrmeister, L., Grosse, G., Fortier, D., Hugelius, G., Knoblauch, C., Romanovsky, V.,
604 Schädel, C., Schneider von Deimling, T., Schuur, E. A. G., Shmelev, D., Ulrich, M. and Veremeeva, A.:
605 Deep Yedoma permafrost: A synthesis of depositional characteristics and carbon vulnerability, Earth-
606 Science Rev., 172, 75–86, doi:10.1016/j.earscirev.2017.07.007, 2017.

607 Treat, C. C., Natali, S. M., Ernakovich, J., Iversen, C. M., Lupascu, M., McGuire, A. D., Norby, R. J., Roy
608 Chowdhury, T., Richter, A., Šantrůčková, H., Schädel, C., Schuur, E. A. G., Sloan, V. L., Turetsky, M. R.
609 and Waldrop, M. P.: A pan-Arctic synthesis of CH_4 and CO_2 production from anoxic soil incubations,
610 Glob. Chang. Biol., 21(7), 2787–2803, doi:10.1111/gcb.12875, 2015.

611 Ulrich, M., Grosse, G., Strauss, J. and Schirrmeister, L.: Quantifying wedge-ice volumes in Yedoma and
612 thermokarst Basin deposits, Permafr. Periglac. Process., 25(3), 151–161, doi:10.1002/ppp.1810, 2014.

613 Vonk, J. E., Sánchez-García, L., van Dongen, B. E., Alling, V., Kosmach, D., Charkin, A., Semiletov, I.
614 P., Dudarev, O. V., Shakhova, N., Roos, P., Eglinton, T. I., Andersson, A. and Gustafsson, Ö.: Activation
615 of old carbon by erosion of coastal and subsea permafrost in Arctic Siberia, Nature, 489(7414), 137–
616 140, doi:10.1038/nature11392, 2012.

617 Waldrop, M. P., Wickland, K. P., White Iii, R., Berhe, A. A., Harden, J. W. and Romanovsky, V. E.:
618 Molecular investigations into a globally important carbon pool: Permafrost-protected carbon in Alaskan
619 soils, Glob. Chang. Biol., 16(9), 2543–2554, doi:10.1111/j.1365-2486.2009.02141.x, 2010.

620 Walter Anthony, K. M., Zimov, S. A., Grosse, G., Jones, M. C., Anthony, P. M., Chapin III, F. S., Finlay,
621 J. C., Mack, M. C., Davydov, S., Frenzel, P. and Frolking, S.: A shift of thermokarst lakes from carbon
622 sources to sinks during the Holocene epoch, Nature, 511(7510), 452–456, doi:10.1038/nature13560,
623 2014.

624 Weiss, N., Blok, D., Elberling, B., Hugelius, G., Jørgensen, C. J., Siewert, M. B. and Kuhry, P.:
625 Thermokarst dynamics and soil organic matter characteristics controlling initial carbon release from
626 permafrost soils in the Siberian Yedoma region, Sediment. Geol., 340, 38–48,
627 doi:10.1016/j.sedgeo.2015.12.004, 2016.

628 Wetterich, S., Kuzmina, S., Andreev, A. A., Kienast, F., Meyer, H., Schirrmeister, L., Kuznetsova, T. and

629 Sierralta, M.: Palaeoenvironmental dynamics inferred from late Quaternary permafrost deposits on
630 Kurungnakh Island, Lena Delta, Northeast Siberia, Russia, Quat. Sci. Rev., 27(15–16), 1523–1540,
631 doi:10.1016/j.quascirev.2008.04.007, 2008.

632 Wetterich, S., Schirrmeister, L., Andreev, A. A., Pudenz, M., Plessen, B., Meyer, H. and Kunitsky, V. V.:
633 Eemian and Late Glacial/Holocene palaeoenvironmental records from permafrost sequences at the
634 Dmitry Laptev Strait (NE Siberia, Russia), Palaeogeogr. Palaeoclimatol. Palaeoecol., 279(1–2), 73–95,
635 doi:10.1016/j.palaeo.2009.05.002, 2009.

636 Wetterich, S., Rudaya, N., Tumskoy, V., Andreev, A. A., Opel, T., Schirrmeister, L. and Meyer, H.: Last
637 Glacial Maximum records in permafrost of the East Siberian Arctic, Quat. Sci. Rev., 30(21–22), 3139–
638 3151, doi:10.1016/j.quascirev.2011.07.020, 2011.

639 Wetterich, S., Tumskoy, V., Rudaya, N., Andreev, A. A., Opel, T., Meyer, H., Schirrmeister, L. and Hüls,
640 M.: Ice Complex formation in arctic East Siberia during the MIS3 Interstadial, Quat. Sci. Rev., 84, 39–
641 55, doi:10.1016/j.quascirev.2013.11.009, 2014.

642 Wetterich, S., Tumskoy, V., Rudaya, N., Kuznetsov, V., Maksimov, F., Opel, T., Meyer, H., Andreev, A.
643 A. and Schirrmeister, L.: Ice Complex permafrost of MIS5 age in the Dmitry Laptev Strait coastal region
644 (East Siberian Arctic), Quat. Sci. Rev., 147, 298–311, doi:10.1016/j.quascirev.2015.11.016, 2016.

645 Willerslev, E., Hansen, A. J., Rønn, R., Brand, T. B., Barnes, I., Wiuf, C., Gilichinsky, D., Mitchell, D. and
646 Cooper, A.: Long-term persistence of bacterial DNA, Curr. Biol., 14(1), R9–R10,
647 doi:10.1016/j.cub.2003.12.012, 2004.

648 Yamamoto, S., Alcauskas, J. B. and Crozier, T. E.: Solubility of methane in distilled water and seawater,
649 J. Chem. Eng. Data, 21(1), 78–80, doi:10.1021/je60068a029, 1976.

650 Zimmermann, H., Raschke, E., Epp, L., Stoof-Leichsenring, K., Schirrmeister, L., Schwamborn, G. and
651 Herzschuh, U.: The history of tree and shrub taxa on Bol'shoy Lyakhovsky Island (New Siberian
652 Archipelago) since the last interglacial uncovered by sedimentary ancient DNA and pollen data, Genes
653 (Basel)., 8(10), 273, doi:10.3390/genes8100273, 2017a.

654 Zimmermann, H. H., Raschke, E., Epp, L. S., Stoof-Leichsenring, K. R., Schwamborn, G., Schirrmeister,
655 L., Overduin, P. P. and Herzschuh, U.: Sedimentary ancient DNA and pollen reveal the composition of
656 plant organic matter in Late Quaternary permafrost sediments of the Buor Khaya Peninsula (north-
657 eastern Siberia), Biogeosciences, 14(3), 575–596, doi:10.5194/bg-14-575-2017, 2017b.

658 Zimov, S. A., Davydov, S. P., Zimova, G. M., Davydova, A. I., Schuur, E. A. G., Dutta, K. and Chapin III,
659 F. S.: Permafrost carbon: Stock and decomposability of a globally significant carbon pool, Geophys. Res.
660 Lett., 33(20), L20502, doi:10.1029/2006GL027484, 2006.

Biogeosciences
Discussions
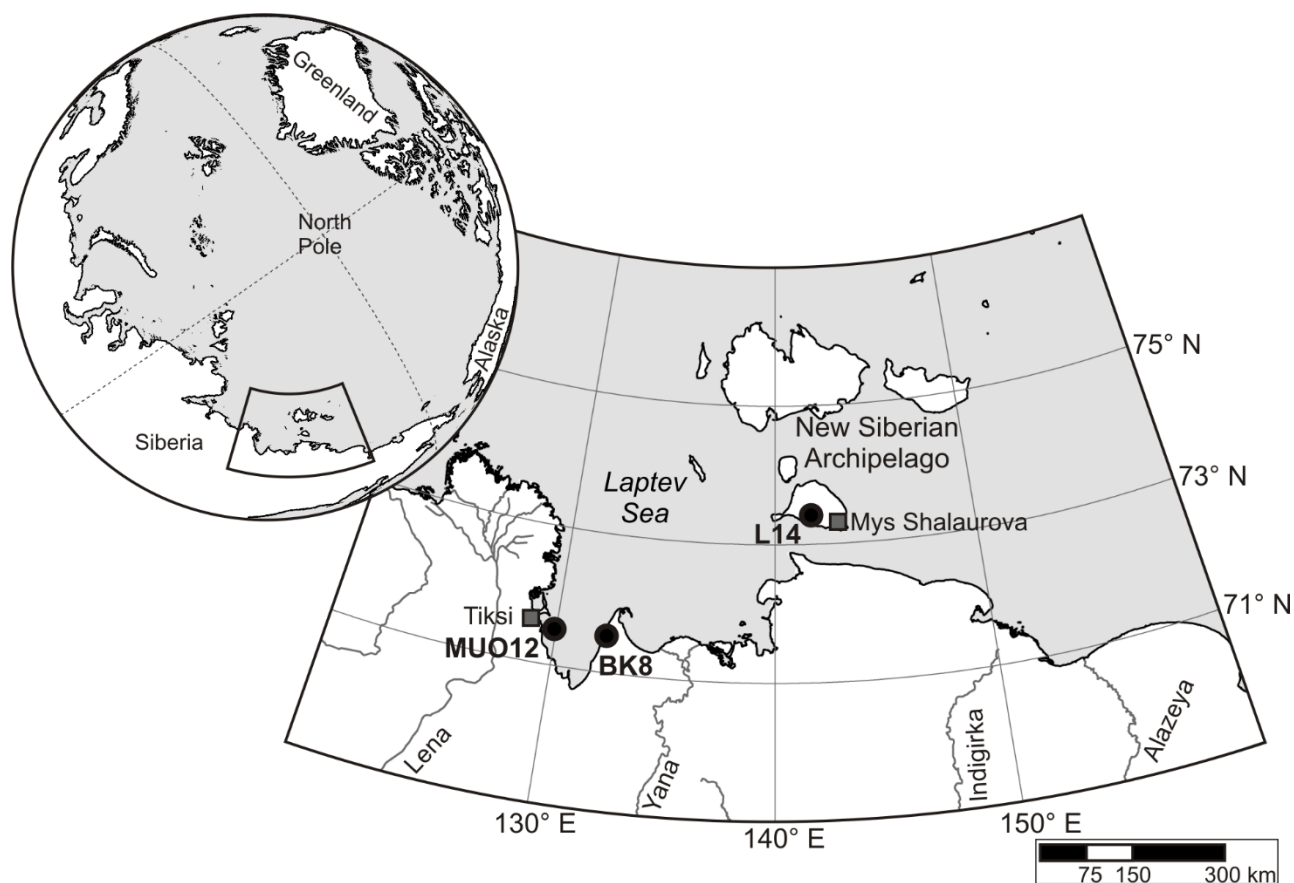
Figures

Figure 1. Overview map of the Laptev Sea region with the study locations at Muostakh Island (sample code MUO12), the Buor Khaya Peninsula (BK8) and Bol'shoy Lyakhovsky Island (L14).
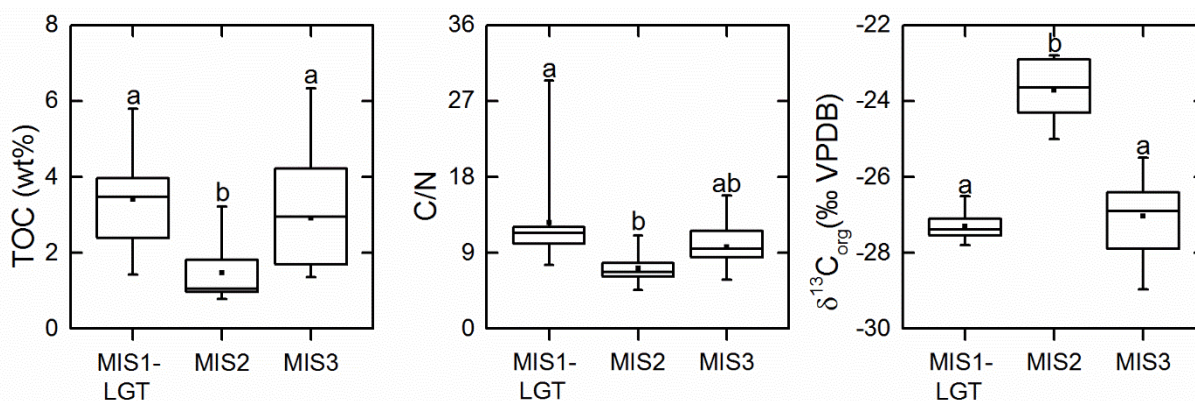
Figure 2. Boxplot of total organic carbon (TOC), total organic carbon to total nitrogen ratio (C/N) and $\delta^{13}C_{org}$-values of permafrost deposits from the MUO12 sequence, the BK8 core, and the two L14 cores

669 from the Holocene interglacial (MIS 1), including the late glacial transition (LGT) (n = 12), the Sartan
670 stadial (MIS 2) (n = 6), and the Kargin interstadial (MIS 3) (n = 27). The whiskers show the data range
671 and the box indicates the interquartile range. The vertical line and square inside the boxes show the
672 median and mean, respectively. The letters above the whiskers indicate statistically significant
673 differences in geochemical characteristics between the deposits of different ages (Mann-Whitney test, p
674 < 0.016 for TOC and C/N, p < 0.001 for $\delta^{13}C_{org}$)
675
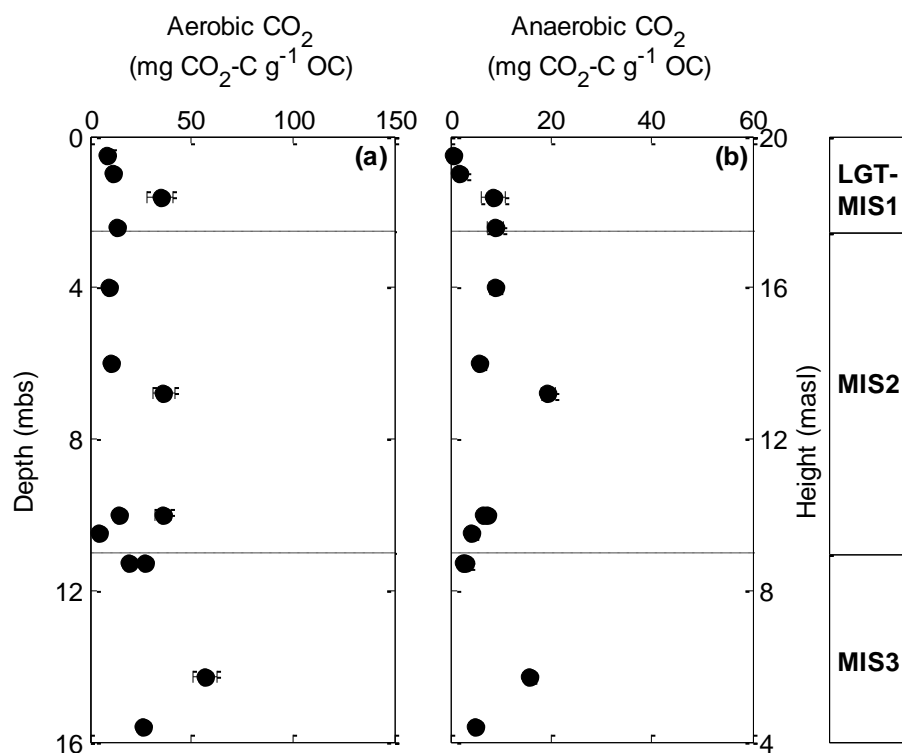
676
677 Figure 3. Depth profiles of total aerobic (a) and anaerobic (b) CO_2 production per gram organic carbon
678 (g^{-1} OC) in sediment samples from the MUO12 sequence after 134 incubation days at 4 °C for deposits
679 from the Holocene interglacial (MIS 1), including the late glacial transition (LGT), the Sartan stadial (MIS
680 2), and the Kargin interstadial (MIS 3). Data are mean values (n = 3) and error bars represent one
681 standard deviation. Note the different scales. No CH_4 production was observed during the 134-days
682 incubation period.
683

684
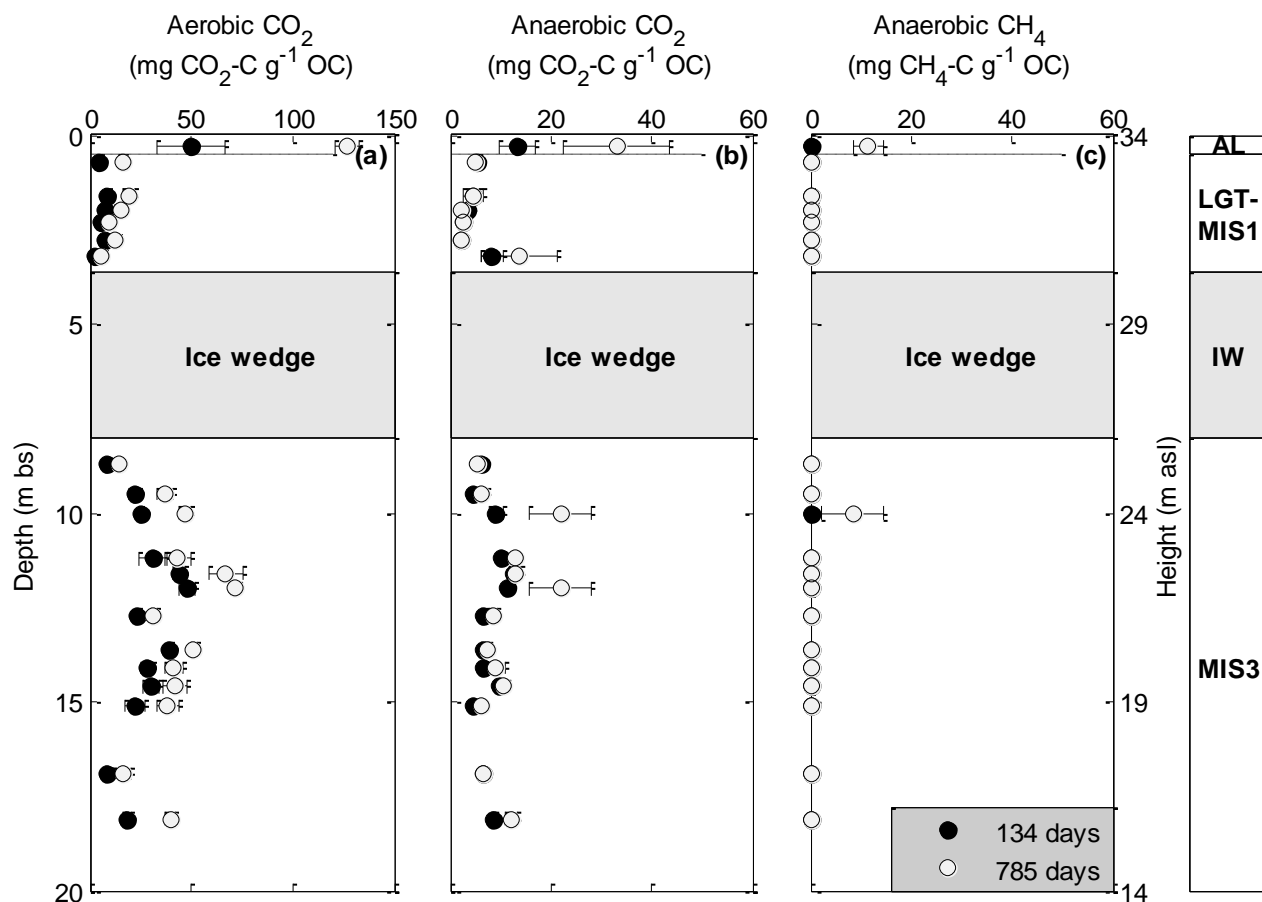
Figure 4. Depth profiles of total aerobic CO_2 (a), anaerobic CO_2 (b) and anaerobic CH_4 (c) production per gram organic carbon (g^{-1} OC) in sediment samples from the BK8 core after 134 (closed symbols) and 785 incubation days (open symbols) at 4 °C for the active layer (AL) and permafrost deposits from the Holocene interglacial (MIS 1), including the late glacial transition (LGT) and the Kargin interstadial (MIS 3). Data are mean values (n = 3) and error bars represent one standard deviation. Note the different scales.

Biogeosciences
Discussions

Open Access

692
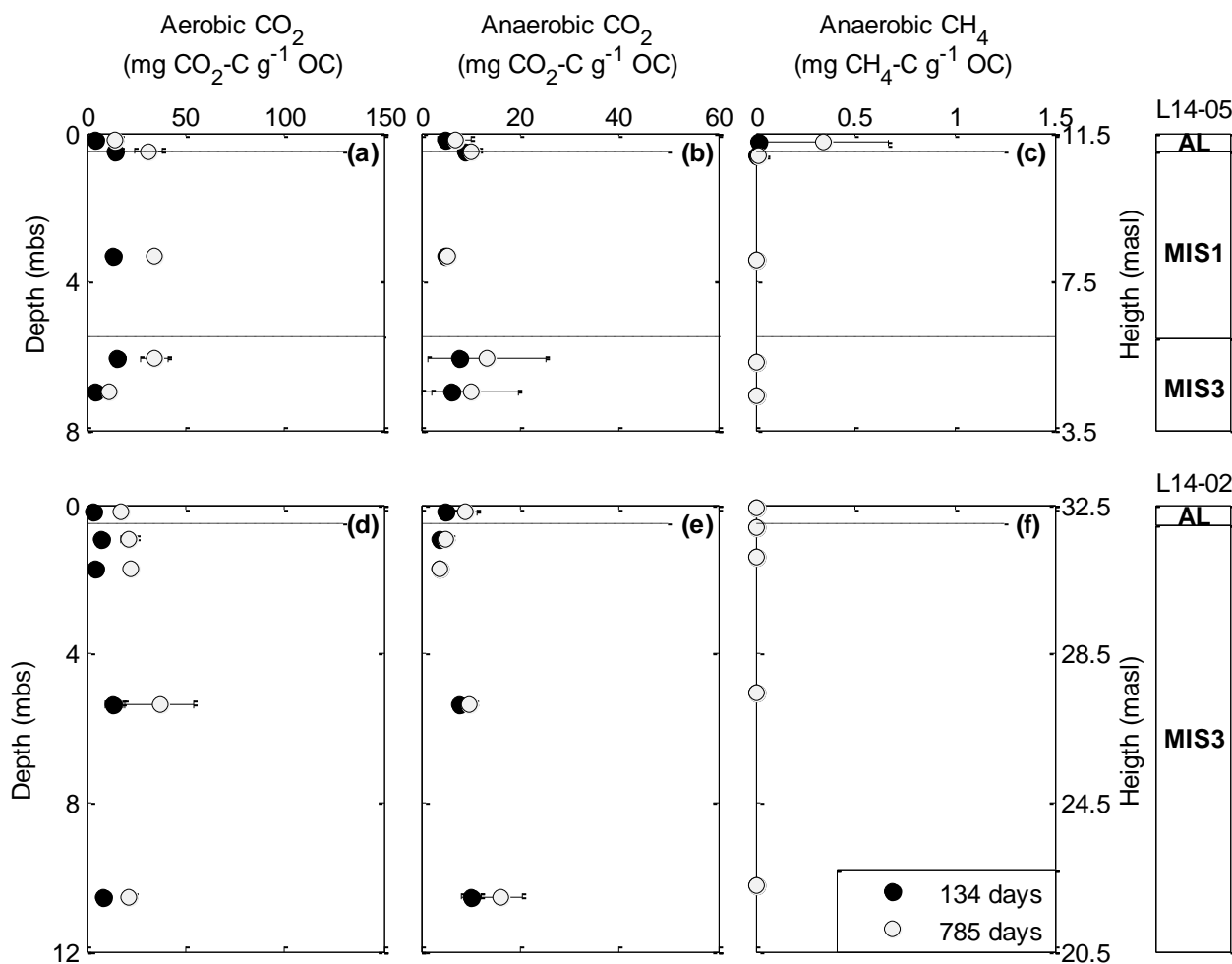
Figure 5. Depth profiles of total aerobic CO_2 (a), anaerobic CO_2 (b) and anaerobic CH_4 (c) production
per gram organic carbon (g^{-1} OC) in sediment samples from the L14-05 (a,b,c), and L14-02 cores (d,e,f)
after 134 (closed symbols) and 785 incubation days (open symbols) at 4 °C for the active layer (AL) and
permafrost deposits from the Holocene interglacial (MIS 1) and the Kargin interstadial (MIS 3). Data are
mean values (n = 3) and error bars represent one standard deviation. Note the different scales.

698

Biogeosciences
Discussions

Open Access

EGU
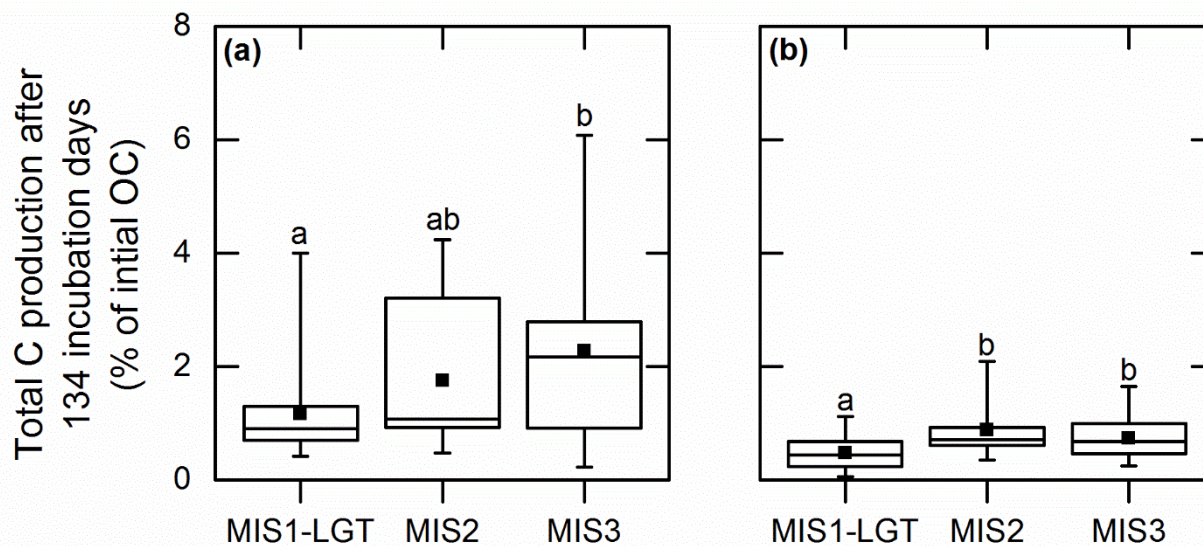
Figure 6. Total aerobic (a) and anaerobic (b) CO_2-C production after 134 incubation days from permafrost deposits from the MUO12 sequence, the BK8 core, and the two L14 cores from the Holocene interglacial (MIS 1), including the late glacial transition (LGT) (n = 22), the Sartan stadial (MIS 2) (n = 15), and the Kargin interstadial (MIS 3) (n = 50). The whiskers show the data range and the box indicates the interquartile range. The vertical line and square inside the boxes show the median and mean, respectively. The different letters indicate significant differences (Mann-Whitney test, $p < 0.016$) between deposits from different periods.

Tables

Table 1. Compilation of the regional chronostratigraphy of the Laptev Sea region used in this work with paleoclimate (summer) and vegetation history based on an overview by Andreev et al. (2011) and references therein.

Age ka BP	Period	Regional chrono-stratigraphy	Marine isotope stage (MIS)	Regional climate and vegetation
<10.3	Holocene	Holocene	MIS 1	Climate amelioration during the early Holocene; shrub-tundra vegetation gradually disappeared ca 7.6 ka BP
ca 10.3–13	Late glacial-early Holocene transition			Climate amelioration after the Last Glacial Maximum; transition to shrubby tundra vegetation
ca 13–30	Late Weichselian glacial (stadial)	Sartan	MIS 2	Cold and dry summer conditions, winter colder than today; open tundra steppe
ca 30–55	Middle Weichselian glacial (interstadial)	Kargin	MIS 3	Relatively warm and wet summers; open herb and shrub dominated vegetation